Phase separation patterns for diblock copolymers on spherical surfaces: A finite volume method

Ping Tang, Feng Qiu,* Hongdong Zhang, and Yuliang Yang
The Key Laboratory of Molecular Engineering of Polymers, Ministry of Education, China and Department of Macromolecular Science, Fudan University, Shanghai 200433, China

(Received 6 January 2005; revised manuscript received 20 April 2005; published 18 July 2005)

We explore phase separation on spherical surfaces by solving the Cahn-Hilliard equation modified for diblock copolymers using a finite volume method. The spherical surface is discretized into almost uniform triangles by employing successive dyadic refinements of the spherical icosahedron, a methodology that avoids potential mathematical and numerical problems related to the poles in spherical coordinates. The finite volume method is based on averaging Voronoi cells built from triangular meshes to calculate the Laplace-Beltrami operator on the curved surface, which greatly improves both the accuracy and speed of calculation as compared to the conventional finite difference method. By using this method we simulate the phase separation of diblock copolymers on a spherical surface. It is found that stable and intrinsic defects, which would not occur in a flat space after sufficient annealing, appear in the periodic arrangement of the domains on the curved surface due to the distinct Euler characteristic of the surface.

DOI: 10.1103/PhysRevE.72.016710 PACS number(s): 05.10.−a, 64.60.Cn

I. INTRODUCTION

Recent experiments demonstrated that phase ordering or phase separation could occur on static or dynamic surfaces. Examples include lipid bilayer membranes [1], crystal growth on curved surfaces [2], and phase separation within thin films [3]. Due to the mathematical and numerical challenges involved, theoretical investigations have been limited and analytical results are derived only for some special classes of surfaces with translation or rotation symmetry, such as surfaces of circular and elliptic cylinders, and tori [4,5]. Actually, in flat spaces the phase ordering processes have been successfully investigated with the Cahn-Hilliard (CH) equation in a wide variety of nonequilibrium systems ranging from binary metal alloys [6] to soft materials such as block copolymers [7]. The numerical implementation of the CH equation has been based on the conventional finite difference method although some special techniques such as the cell dynamics scheme [8] are often adopted to speed up the simulation.

The simulation of phase separation kinetics in spherical geometry is a difficult problem and only a few numerical studies deal with surfaces that have the topology of a sphere by using finite difference [9]. Recently, Varea *et al.* studied the pattern formation on the spherical surface based on Turing equations [10]. The key point to extend the CH equation in flat space to that on the sphere is how to calculate the Laplace-Beltrami operator for describing the Laplacian on the curved surface. Therefore, we concentrate on presenting a numerical implementation of the Laplace-Beltrami operator on the spherical surface with triangular lattice discretization. In this paper, a numerical algorithm is based upon a spatial triangular discretization derived from the regular icosahedron and employs the finite volume method which can facilitate the investigation of phase ordering processes on rigid surfaces with spherical topology. By solving the CH equation using this method, we simulate the phase separation morphology of diblock copolymers on a spherical surface. Our results show that for both symmetric and asymmetric composition, stable and intrinsic defects, which would not occur in a flat space after sufficient annealing, appear in the lamellae and spherical phase on the curved surface due to the distinct Euler characteristic of the surface. Compared to the conventional finite difference method, our methodology by means of the finite volume based on averaging Voronoi cells demonstrates great potential to implement numerical solving of the CH equation for describing phase separation dynamics on the curved surface, especially spherical surface.

II. THEORETICAL MODEL

In this section, we first briefly review the simplest dissipative model conventionally known as the Cahn-Hilliard equation or model B in the Hohenberg-Halperin notation [11,12], for describing phase separation kinetics of *AB* diblock copolymers in the flat space, and then describe extensions of the model in the curved space. The CH equation in the flat space is written as [11,12]

$$\frac{\partial \varphi}{\partial t} = M\nabla^2\left(\frac{\delta F(\varphi)}{\delta \varphi}\right) \tag{1}$$

where M is the mobility, and the order parameter φ is defined as the local difference between the concentrations of the two components A and B, i.e., $\varphi=2\phi-1$ (ϕ is the volume fraction of the A component of the AB diblock copolymer). $F(\varphi)$ is the free energy functional, which has the following form [13,14]:

*Author to whom correspondence should be addressed. Electronic address: fengqiu@fudan.edu.cn

$$\frac{F[\varphi(\mathbf{r})]}{k_BT} = \int d\mathbf{r}\left\{ f[\varphi(\mathbf{r})] + \frac{k}{2}|\nabla\varphi(\mathbf{r})|^2 + \frac{\alpha}{2}\int d\mathbf{r} \times \int d\mathbf{r}' G(\mathbf{r}-\mathbf{r}')[\varphi(\mathbf{r})-\bar{\varphi}][\varphi(\mathbf{r}')-\bar{\varphi}]\right\} \quad (2)$$

where k_B is the Boltzmann constant, T is the temperature, $\mathbf{r}$ is the position vector, and $f(\phi)$ is the local coarse-grained free energy of mixing. $f(\varphi)$ takes the Landau form in this work: $f(\varphi)=-\varphi^2/2+\varphi^4/4$. The first and second terms in Eq. (2) represent the short-range repulsive interaction between the A and B species, and the third term represents the long-range interaction due to the connection of the A and B blocks. G is the Green's function that satisfies $\nabla^2 G(\mathbf{r},\mathbf{r}')=-\delta(\mathbf{r}-\mathbf{r}')$, and $\bar{\varphi}$ is the spatially averaged order parameter. $\alpha \propto 1/[N^2 f(1-f)]$ is a phenomenological parameter, where N and f are the chain length and composition of the diblock, respectively. Substituting Eq. (2) into Eq. (1) and rescaling it with M leads to the CH equation for an AB diblock copolymer in the flat space:

$$\frac{\partial\varphi}{\partial t} = \nabla^2[-\varphi+\varphi^3-\nabla^2\varphi] - \alpha(\varphi-\bar{\varphi}). \quad (3)$$

It is noted that Eq. (3) modeling microphase separation results in an equation identical in form to that used to describe spinodal decomposition in the presence of simple chemical reaction [15].

A two-dimensional (2D) closed spherical surface embedded in a 3D space is denoted by the curvilinear coordinate $\{u\}=\{u^1,u^2\}$. A position vector at a time t of a point at the surface specified by $\{u\}=\{u^1,u^2\}$ can be expressed as $\mathbf{r}=\mathbf{r}\{u^1,u^2,t\}$. In order to extend the CH equation in the flat space [Eq. (3)] to that on the curved surface, the ∇^2 should be replaced by the covariant Laplacian ∇^2_{LB}, also known as the Laplace-Beltrami operator, which is used as the Laplacian on curved surfaces [16]:

$$\nabla^2_{LB}X = g^{\alpha\beta}X_{,\alpha}|_\beta = g^{\alpha\beta}(X_{,\alpha\beta}-\Gamma^\gamma_{\alpha\beta}X_{,\gamma}) \quad (4)$$

where X is the value of a field, such as concentration or chemical potential field, $X_{,\alpha}=\partial X(u)/\partial u^\alpha$, and $X_{,\alpha\beta}=\partial^2 X(u)/\partial u^\alpha \partial u^\beta$. $X_{,\alpha}|_\beta$ is the covariant derivative and can be written as $X_{,\alpha}|_\beta = X_{,\alpha\beta}-\Gamma^\gamma_{\alpha\beta}X_{,\gamma}$. $g_{\alpha\beta}$ is the metric tensor and is given by

$$g_{\alpha\beta} = \mathbf{g}_\alpha\cdot\mathbf{g}_\beta = \partial\mathbf{r}/\partial u^\alpha\cdot\partial\mathbf{r}/\partial u^\beta \quad (5)$$

where $\mathbf{g}_\alpha$ and $\mathbf{g}_\beta$ are tangential vectors. $g^{\alpha\beta}$ is the contravariant metric tensor, $g^{\alpha\beta}=(g_{\alpha\beta})^{-1}$. The Christoffel symbol $\Gamma^\gamma_{\alpha\beta}$ is

$$\Gamma^\gamma_{\alpha\beta} = \frac{1}{2}g^{\gamma\xi}\left(\frac{\partial g_{\alpha\xi}}{\partial u^\beta}+\frac{\partial g_{\beta\xi}}{\partial u^\alpha}-\frac{\partial g_{\alpha\beta}}{\partial u^\xi}\right). \quad (6)$$

We take the Einstein summation notation for the repeated alternate Greek indices ($\alpha,\beta,\gamma,\xi=1,2$, denoting curvilinear coordinates u^1 and u^2, respectively). For example, Eq. (4) is expressed as

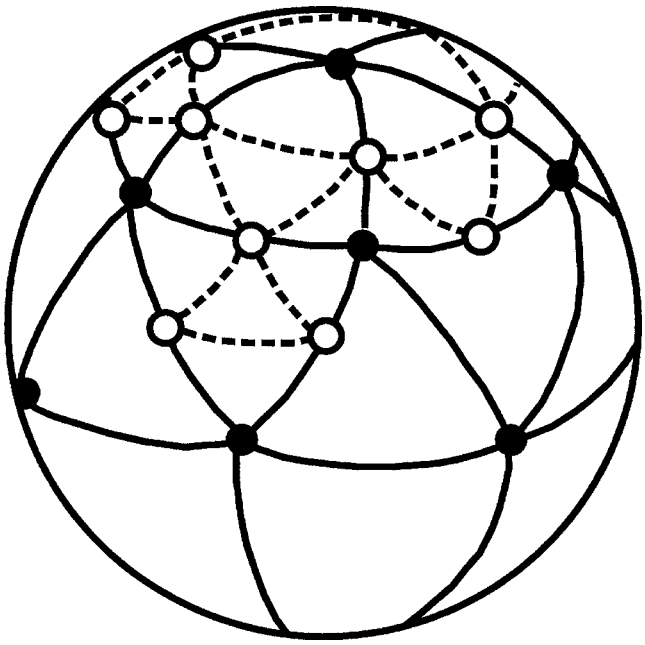

FIG. 1. The schematic of dyadic icosahedral triangulation of a spherical surface.

$$\begin{aligned}\nabla^2_{LB}X = g^{\alpha\beta}(X_{,\alpha\beta}-\Gamma^\gamma_{\alpha\beta}X_{,\gamma}) &= g^{11}(X_{,11}-X_{,1}\Gamma^1_{11}-X_{,2}\Gamma^2_{11}) \\ &+ g^{21}(X_{,21}-X_{,1}\Gamma^1_{21}-X_{,2}\Gamma^2_{21}) \\ &+ g^{12}(X_{,12}-X_{,1}\Gamma^1_{12}-X_{,2}\Gamma^2_{12}) \\ &+ g^{22}(X_{,22}-X_{,1}\Gamma^1_{22}-X_{,2}\Gamma^2_{22}). \end{aligned} \quad (7)$$

The CH equation for AB diblock copolymers on a curved surface is therefore given by

$$\frac{\partial\varphi}{\partial t} = \nabla^2_{LB}[-\varphi+\varphi^3-\nabla^2_{LB}\varphi] - \alpha(\varphi-\bar{\varphi}). \quad (8)$$

The key to solve Eq. (8) involves evaluating the Laplace-Beltrami operator on a curved surface. In the next section, we present the finite volume method to numerically calculate the Laplace-Beltrami operator on a rigid spherical surface with a triangular lattice.

III. NUMERICAL IMPLEMENTATION

A. Discretization of the spherical surface

The spherical surface is spatially discretized with nearly uniform triangular lattices to numerically solve the CH equation. The spherical surface is first discretized into triangular grids generated by the spherical projection of the regular icosahedron [17], i.e., a structure like the backbone of C_{60} fullerene [18], which consists of 20 equal spherical triangles and 12 vertices, as shown in Fig. 1. When the midpoints (empty dots) of three edges with geodesic arcs are connected by a line (indicated by dotted lines in Fig. 1), each of the 20 triangular faces is subdivided into four, yielding 80 smaller triangles. Repeating such a dyadic subdivision, higher order triangulation and finer grids can be obtained in this simple procedure. In such triangular lattice, each vertex has six

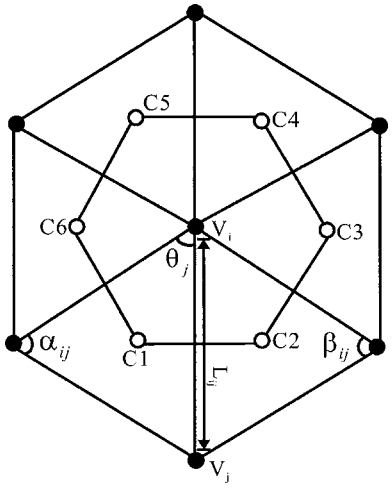

FIG. 2. A vertex with six neighbors and one-ring Voronoi region for evaluating the Laplace-Beltrami operator on a spherical surface.

neighbors, except for those 12 singular vertices that belong to the original spherical icosahedron, which has five neighbors each. In fact, a classic theorem of Euler shows that any triangulation of the sphere surface must exist in excess of exactly 12 fivefold coordinated vertices [2,19]. In this paper, the sphere surface is triangulated with $N=12\,962$ ($N=10n^2+2$, where n is an arbitrary integer) vertices and the radius of the sphere is set to be 31.25 to keep the lattice size (space step) to be about 1 for the aim of numerical stability.

B. Solving CH equation on the surface lattice

We now present a finite volume algorithm to calculate the Laplace-Beltrami operator of a field $\nabla^2_{LB}X$, i.e., the Laplacian of a curved surface, in terms of the above triangulation. This algorithm is based upon averaging Voronoi cells, which was presented by Meyer *et al.* in a different context [20]. As shown in Fig. 2, the Laplace-Beltrami operator at each vertex can be defined as the average over the immediate one-ring neighboring triangles. For each vertex, an associated surface patch is chosen, which is the so-called Voronoi cell or finite volume. In the Voronoi area, the piecewise linear boundaries connect the midpoints of the edges emanating from the center vertex and a point, which is the circumcenter of each adjacent triangle. The value of the Laplace-Beltrami operator of a field X at a vertex i can be expressed as a function of the field values of the nodes and the angles of the triangulation:

$$\nabla^2_{LB}X = \frac{1}{2A_{\text{Voronoi}}} \sum_{j\in V_1(i)} (\cot \alpha_{ij} + \cot \beta_{ij})(X_j - X_i) \quad (9)$$

where α_{ij} and β_{ij} are two angles opposite to the edges in two triangles sharing the edge. X_i and X_j are the field values at the vertex i and j. $V_1(i)$ is the set of one ring of neighbor vertices of vertex V_i. A_{Voronoi} is the area of the one-ring Voronoi region, which is enclosed by the points C_1, C_2, C_3, C_4, C_5, and C_6, as shown in Fig. 2. A_{Voronoi} is obtained:

$$A_{\text{Voronoi}} = \frac{1}{8} \sum_{j\in V_1(i)} (\cot \alpha_{ij} + \cot \beta_{ij})(L_{ij})^2. \quad (10)$$

TABLE I. A comparison of the accuracy between the finite difference and finite volume methods.

% error	Finite difference	Finite volume
Mean curvature	0.11	0.0062
Gaussian curvature	0.23	0.024
Total surface area	0.093	0.023

According to the finite volume method, the mean curvature $H(V_i)$ and Gauss curvature $K(V_i)$ at a vertex V_i are respectively written as

$$H(V_i) = \frac{1}{4A_{\text{Voronoi}}} \sum_{j\in V_1(i)} (\cot \alpha_{ij} + \cot \beta_{ij})L_{ij}, \quad (11)$$

$$K(V_i) = \frac{1}{A_{\text{Voronoi}}} \left(2\pi - \sum_{j=1}^{\mathcal{N}(f)} \theta_j \right) \quad (12)$$

where θ_j is the angle of the jth face at the vertex V_i, and $\mathcal{N}(f)$ denotes the number of faces around this vertex V_i.

Comparing the finite volume method to discretize the Laplace-Beltrami operator on curved surfaces with the conventional finite difference in the Appendix, it is clear that the former is quite simple and straightforward to implement. In particular, the major advantage of this method is its suitability for an arbitrary triangle mesh regardless of whether the vertex has six or five neighbors. Table I lists the typical numerical quality of the two methods in terms of the curvatures and area of the sphere surface, as the analytical results of these quantities are known. The result listed in Table I clearly shows that the numerical quality of the finite volume method is quite good and is better than the finite difference method. Furthermore, the speed of calculation of these two methods is compared for simulating a same phase separation process (as will be presented in Sec. III C), the finite volume method is at least three times faster than the finite difference method. However, the finite difference method can be used to evaluate the first and second order difference of the field defined on the surface with respect to curvilinear coordinates [Eqs. (A2)–(A7)], while the finite volume method is not easy to deal with this.

C. Numerical results

The time evolution of morphology of *AB* diblock copolymers on a rigid spherical surface is shown in Fig. 3, using the finite volume method. The order parameter $\varphi=2\phi-1$ is defined as the local volume fraction difference of components *A* and *B*. The *A*- and *B*-rich regions are shown by bold and light dots, respectively. At early stages of microphase separation, randomly distributed *A* and *B* domains are observed; however, at later stages a stable, periodic lamellar phase is formed because of the symmetric composition ($\phi=0.5$). In particular, both the *A* and *B* lamellae display spiral structures on the surface of the sphere, which is not observed to occur in flat space. Similar spiral waves were also observed by Gomatam *et al.* in a reaction-diffusion system on a sphere

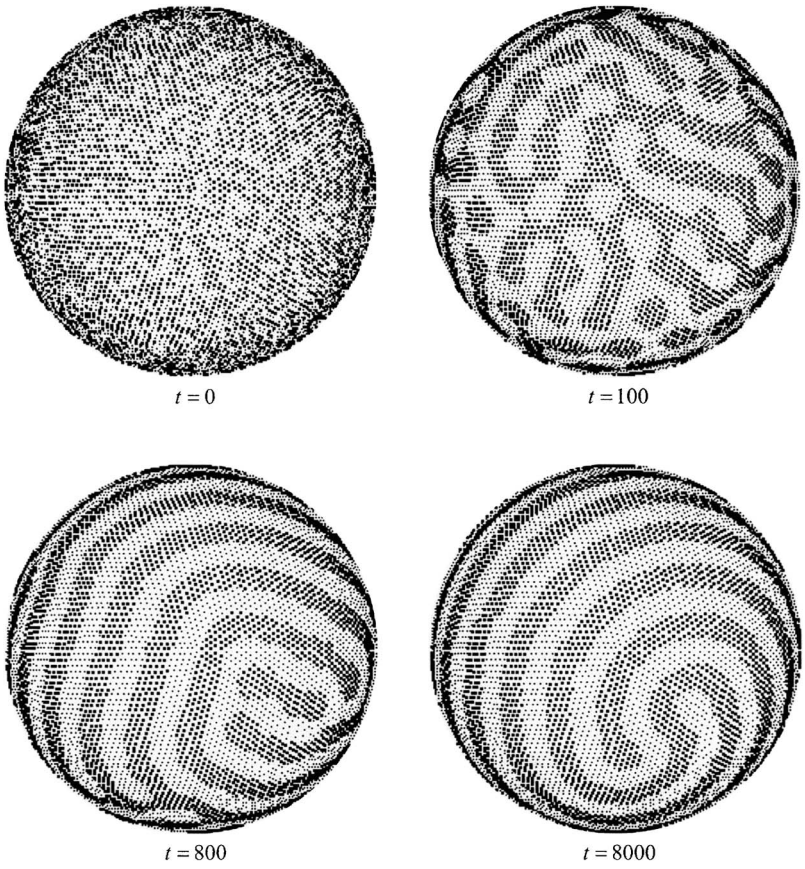

FIG. 3. The evolution of morphologies with time t for AB diblock copolymers with the copolymer composition $\phi=0.5$ and $\alpha=0.2$.

surface [21]. It is interesting to see that four disclinations of type 1/2 emerge in the area where the spiral tips locate, in which one disclination produced by the A lamellae is paired with that produced by the B lamellae, and the two pairs are located at the opposite poles of the sphere surface. Actually, a very similar pattern on the sphere with the same pair of 1/2 disclinations in the study of Turing patterns was reported by Varea and his co-workers [10]. Furthermore, it is worth noting that similar disclinations could appear in a nematically ordered phase on sphere surfaces, with the four disclinations located at the vertices of a tetrahedron [22], which is different from the lamellar case studied here. These results suggest that these defects are intrinsic and stable and thereby cannot be removed by annealing for even longer time.

Figure 4 shows the time evolution of the microphase for an asymmetric diblock copolymer with the composition $\phi=0.35$. From a random initial state, the system microphase separates into a spherical phase with the minority component A forming spheres while the majority component B forming the matrix. Note that at later stages the A forming spheres are arranged in an almost hexagonal pattern, in which most of the A spheres have six nearest neighbors while some of them only have five nearest neighbors. Like the disclinations observed in the symmetric case, these defects are stable and cannot be removed by annealing for longer time. Actually, recent experimental and theoretical results demonstrated that the arrangement of the ordered structure on the surface of the sphere must lead to the similar defects [2,23].

Furthermore, the phase separation kinetics of polymer blends on the spherical surface is also studied and the domain growth law at the late stage of phase separation on the sphere is compared with that in the usual flat space as we take $\alpha=0$ in Eq. (3). The domain growth indicated by the number of lattice points N_B located at domain boundaries which is proportional to the total length of boundaries is shown with time evolution during phase separation in Fig. 5. The results indicate that in the late stage of both symmetric and asymmetric phase separation, when the domain size is not large enough to be affected by the non-Euclidean geometry, we obtain the growth law $N_B \propto t^{-1/3}$, as expected from evaporation-condensation mechanism derived in the flat space proposed by Lifshitz and Slyozov [24]. However, at the very late stage, i.e., when the domains are large enough to "feel" curve characteristics of the sphere, our numerical fitting routine does not provide a reasonable Lifshitz-Slyozov power law fit and no clear value of the exponent can be extracted especially for the case of off-critical quench. The results suggest that the geometrical topology may play an important role in domain growth law during the fairly late stage of phase separation.

Finally, the last term at the right hand side of Eq. (3) represents the long-range interaction due to the chemical bonds of the A and B blocks. The phenomenological parameter α is inversely proportional to N, i.e., the smaller α, the stronger the microphase segregation degree between blocks A and B. However, when α is too small ($\alpha \to 0$), the term of long-range interaction will disappear and thus the microphase separation does not take place. On the other hand, when the value of α is very large the microphase separation does not occur either and the system is in disorder in this

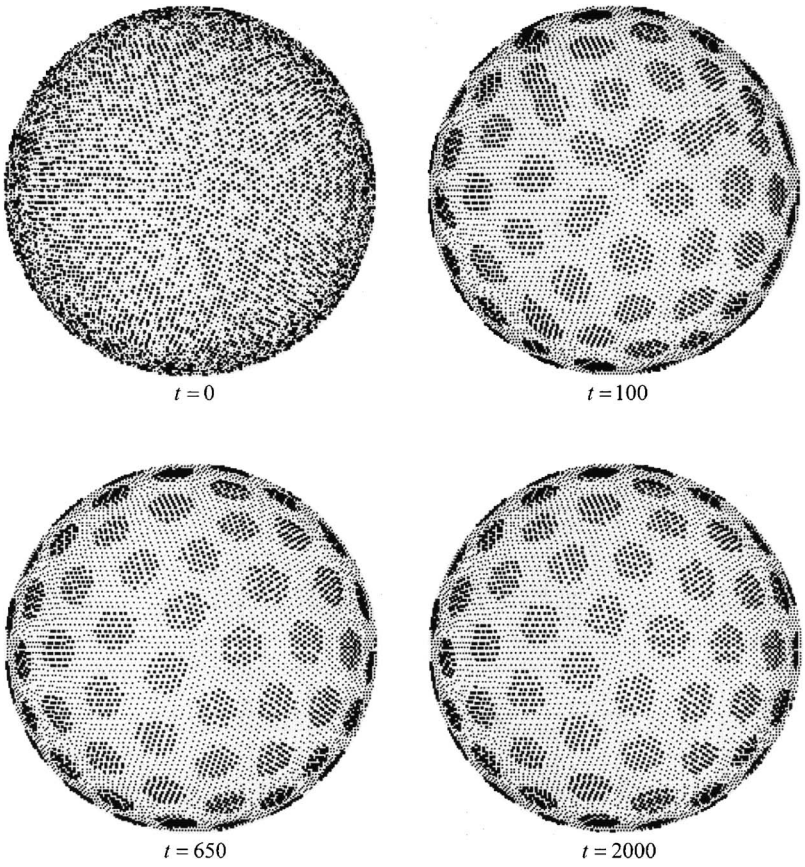

FIG. 4. The time evolution of morphologies for *AB* diblock copolymers with the copolymer composition $\phi=0.35$ and $\alpha=0.1$.

case. For example, for symmetric composition quench, when $\alpha>0.25$ and $\alpha<0.01$ the long-range interaction does not take effect at all and thus the microphase separation cannot be observed.

IV. CONCLUSIONS

We have presented a finite volume method for solving the CH equation on spherical surfaces with icosahedral triangulation, which is based on averaging Voronoi cells to calculate the Laplace-Beltrami operator. Compared to the conventional finite difference method, the finite volume method greatly improves both the accuracy and speed of calculation. This method is then applied to simulate the time evolution of the morphology of *AB* diblock copolymers on a rigid spherical surface. In the late stage of the phase separation, for the symmetric composition of the block copolymers, spiral structures of both the *A* and *B* lamellae are found on the surface of the sphere, which is not observed to occur in flat space; For the spherical phase with asymmetric composition, however, stable defects that cannot be removed by annealing are observed in a hexagonal lattice on the sphere surface. The disclinations formed in the lamellar phase and the defects in the spherical phase are intrinsic in the phase separation of diblock copolymers on sphere surfaces. The dependence of the type and number of these defects with respect to the sphere radius, the polymer chain length and composition, as well as the segregation parameter will be the subject of a future publication.

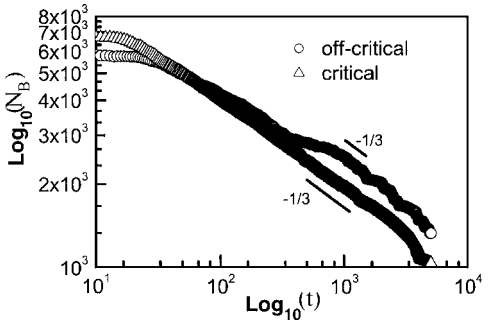

FIG. 5. Log-log plots of N_B representing the domain size as a function of time t for polymer blends. The guide line is $N_B \sim t^{-1/3}$.

ACKNOWLEDGMENTS

We are grateful to Dr. T. Taniguchi for invaluable assistance in relation to the implementation of the finite difference method that we employed herein. We gratefully acknowledge financial support from the NSF of China (Grants No. 20104002, No. 20234010, No. 20474012, No. 20374016, and No. 20221402, and Grant for Excellent Research Group No. 20221402). F.Q. acknowledges support from the Ministry of Education of China (FANEDD 200225) and STCSM (Grant No. 02QE14010).

APPENDIX

The finite difference method is based upon the application of the conventionally finite difference approximation to tri-

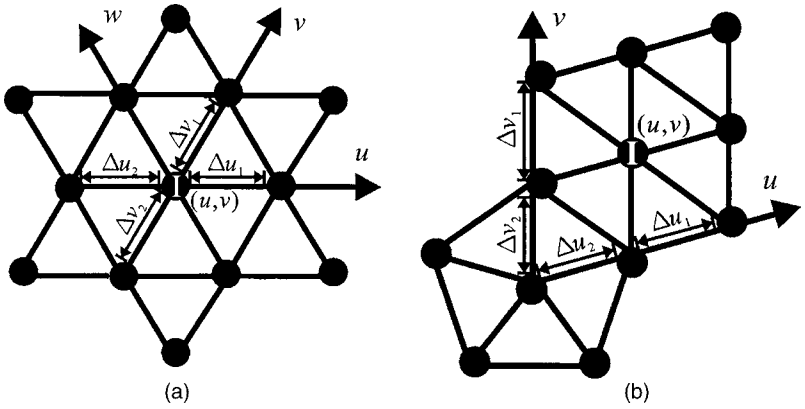

FIG. 6. Lattice points used to calculate $X_{,\alpha}=\partial X(u)/\partial u^{\alpha}$ and $X_{,\alpha\beta}=\partial^2 X(u)/\partial u^{\alpha}\partial u^{\beta}$ for the vertex with (a) six and (b) five neighbors.

angle meshes. According to Eq. (7), the metric tensor $g_{\alpha\beta}$ and its partial derivative with respect to the curvilinear coordinate, $\partial g_{\alpha\beta}/\partial u^{\gamma}$, are required to calculate the Laplace-Beltrami operator. According to Eqs. (5) and (6), one should calculate the first and second order partial derivatives of the position vector $\mathbf{r}$ with respect to the curvilinear parameters $\{u^1,u^2\}$. For convenience, we denote $u^1=u$, $u^2=v$. The position vector $\mathbf{r}$ at a vertex of the surface specified by $\{u\}=\{u,v\}$ can be expressed as $\mathbf{r}=\mathbf{r}\{u\}=\mathbf{r}(x,y,z)$, where x, y, and z are the corresponding Euclidean coordinates, which are functions of u and v. From Fig. 1, each vertex has six neighbor points except the 12 singular points, and thus the curvilinear parameters u and v can be chosen as the discretization scheme shown in Fig. 6, i.e., for each triangle of the mesh, the triangle itself defines the local surface metric. We consider the expressions for $\partial\mathbf{r}/\partial u^{\alpha}$, $\partial^2\mathbf{r}/\partial(u^{\alpha})^2$, and $\partial^2\mathbf{r}/\partial u^{\alpha}\partial u^{\beta}$ on the spherical surface as shown in Fig. 6. According to the definition of $\mathbf{g}_{\alpha}$ the tangential vector at a vertex is given by

$$\boldsymbol{g}_{\alpha}=\partial\boldsymbol{r}/\partial u^{\alpha}=(\partial x/\partial u^{\alpha},\partial y/\partial u^{\alpha},\partial z/\partial u^{\alpha}). \tag{A1}$$

$\partial^2\boldsymbol{r}/\partial(u^{\alpha})^2$ and $\partial^2\boldsymbol{r}/\partial u^{\alpha}\partial u^{\beta}$ can be written in the same fashion. For a vertex with six neighbors, using the second order central difference approximation, the first and second order partial derivatives of an arbitrary quantity defined at a vertex, say I in Fig. 6(a), with respect to curvilinear parameters are given as follows:

$$\frac{\partial x(u,v)}{\partial u}=\frac{2}{\Delta u_1\Delta u_2(\Delta u_1+\Delta u_2)}\left(\frac{1}{2}(\Delta u_2)^2x(u+\Delta u_1,v)+\frac{1}{2}[-(\Delta u_2)^2+(\Delta u_1)^2]x(u,v)-\frac{1}{2}(\Delta u_1)^2x(u-\Delta u_2,v)\right), \tag{A2}$$

$$\frac{\partial^2 x(u,v)}{\partial u^2}=\frac{2}{\Delta u_1\Delta u_2(\Delta u_1+\Delta u_2)}[\Delta u_2x(u+\Delta u_1,v)-(\Delta u_1+\Delta u_2)x(u,v)+\Delta u_1x(u-\Delta u_2,v)], \tag{A3}$$

$$x_{,uv}(u,v)=\frac{\partial x^2(u,v)}{\partial u\,\partial v}=\frac{2}{\Delta v_1\Delta v_2(\Delta v_1+\Delta v_2)}\left(\frac{1}{2}(\Delta v_2)^2x_{,u}(u,v+\Delta v_1)+\frac{1}{2}[-(\Delta v_2)^2+(\Delta v_1)^2]x_{,u}(u,v)-\frac{1}{2}(\Delta v_1)^2x_{,u}(u,v-\Delta v_2)\right), \tag{A4}$$

where Δu_1, Δu_2, Δv_1, and Δv_2 are spatial units (the arc length between two vertices), which are schematically shown in Fig. 6(a). It is obvious that when $\Delta u_1=\Delta u_2$ and $\Delta v_1=\Delta v_2$, the above central difference formulas are simplified to the usual ones with equal spatial units.

For the case of the vertex with five triangular neighbors, say I in Fig. 6(b), a forward difference formula is used to numerically evaluate the above mentioned first and second order partial derivatives:

$$\frac{\partial x(u,v)}{\partial u}=-\frac{2\Delta u_2+\Delta u_1}{\Delta u_2(\Delta u_1+\Delta u_2)}x(u,v)+\frac{\Delta u_1+\Delta u_2}{\Delta u_1\Delta u_2}x(u+\Delta u_2,v)-\frac{\Delta u_2}{\Delta u_1(\Delta u_1+\Delta u_2)}X(u+\Delta u_1+\Delta u_2,v), \tag{A5}$$

$$\frac{\partial^2 x(u,v)}{\partial u^2}=\frac{2}{\Delta u_2(\Delta u_1+\Delta u_2)}x(u,v)-\frac{2}{\Delta u_1\Delta u_2}x(u+\Delta u_2,v)+\frac{2}{\Delta u_1(\Delta u_1+\Delta u_2)}x(u+\Delta u_1+\Delta u_2,v), \tag{A6}$$

$$x_{,uv}=-\frac{2\Delta v_2+\Delta v_1}{\Delta v_2(\Delta v_1+\Delta v_2)}x_{,u}(u,v)+\frac{\Delta v_1+\Delta v_2}{\Delta v_1\Delta v_2}x_{,u}(u,v+\Delta v_2)-\frac{\Delta v_2}{\Delta v_1(\Delta v_1+\Delta v_2)}x_{,u}(u,v+\Delta v_1+\Delta v_2). \tag{A7}$$

In a similar way, $\partial x(u,v)/\partial v$, $\partial^2 x(u,v)/\partial v^2$, and $x_{,vu}(u,v)$ can be obtained. Finally, we note that due to the nonorthogo-

nality of curvilinear coordinates u and v, $x_{,uv}(u,v)$ and $x_{,vu}(u,v)$ are not exactly equal numerically, although they should be the same in definition. Therefore, the numerical value of $\partial x^2(u,v)/\partial u\,\partial v$ for each vertex should be set as the average, i.e., $\partial x^2(u,v)/\partial u\,\partial v=\frac{1}{2}[x_{,uv}(u,v)+x_{,vu}(u,v)]$, for numerical stability. With Eqs. (A2)–(A7), in a similar way, we can calculate $X_{,\alpha}=\partial X(u)/\partial u^{\alpha}$, $X_{,\alpha\beta}=\partial^2 X(u)/\partial u^{\alpha}\,\partial u^{\beta}$, as well as the tangential vector at a vertex according to the definition of g_{α} [Eq. (A1)]. Therefore, the covariant metric tensor $g_{\alpha\beta}$ can be obtained from the values of g_{α} at a vertex. For example,

$$g_{11}=\boldsymbol{g}_1\cdot\boldsymbol{g}_1=[\partial x(\{u\})/\partial u]^2+[\partial y(\{u\})/\partial u]^2+[\partial z(\{u\})/\partial u]^2. \tag{A8}$$

The calculation of the values of g_{22}, g_{12}, and $g_{21}(g_{12}=g_{21})$ should be straightforward. The mean curvature H and Gauss curvature K at a vertex are, respectively, given by

$$H=\mathrm{Tr}(b_{\alpha}^{\beta})=b_{\alpha}^{\alpha}=g^{\alpha\beta}b_{\alpha\beta}, \tag{A9}$$

$$K=\det(b_{\alpha}^{\beta})=\det(b_{\alpha\gamma}g^{\gamma\beta}), \tag{A10}$$

where $b_{\alpha\beta}$ is the coefficients of the second fundamental form for the curved surface:

$$b_{\alpha\beta}=\mathbf{g}_{\alpha,\beta}\cdot\mathbf{n}. \tag{A11}$$

From Eq. (7), in curved space the Laplacian of a field at a vertex can be obtained numerically, since $g_{\alpha\beta}$, $X_{\alpha\beta}$, X_{γ}, and $\Gamma_{\alpha\beta}^{\gamma}$ have been evaluated in terms of Eqs. (6) and (A1)–(A8). With the same procedure, we can calculate the chemical potential μ at each lattice point and their Laplace-Beltrami values $\nabla_{LB}^2\mu$.

[1] T. Baumgart, S. T. Hess, and W. W. Webb, Nature (London) **425**, 821 (2003).
[2] A. R. Bausch *et al.*, Science **299**, 1716 (2003).
[3] P. Sens and S. A. Safran, Eur. Phys. J. E **1**, 237 (2000).
[4] Y. Jiang, T. Lookman, and A. Saxena, Phys. Rev. E **61**, R57 (2000).
[5] Y. Jiang, T. Lookman, and A. Saxena, Biophys. J. **78**, 1068 (2000).
[6] J. W. Cahn, J. Chem. Phys. **42**, 93 (1965).
[7] S. R. Ren and I. W. Hamley, Macromolecules **34**, 116 (2001).
[8] Y. Oono and S. Puri, Phys. Rev. Lett. **58**, 836 (1987).
[9] T. Taniguchi, Phys. Rev. Lett. **76**, 4444 (1996).
[10] C. Varea, J. L. Aragon, and R. A. Barrio, Phys. Rev. E **60**, 4588 (1999).
[11] P. C. Hohenberg and B. I. Halperin, Rev. Mod. Phys. **49**, 435 (1976).
[12] J. D. Gunton, M. M. San, and P. Sahni, in *Phase Transitions and Critical Phenomena*, edited by C. Domb and J. L. Lebowitz (Academic, New York, 1983), Vol. 8.
[13] L. Leibler, Macromolecules **13**, 1602 (1980).
[14] T. Ohta and K. Kawasaki, Macromolecules **19**, 2621 (1986).
[15] S. Puri and H. L. Frisch, J. Phys. A **27**, 6027 (1994).
[16] Z. C. Ou-Yang, J. X. Liu, and Y. Z. Xie, in *Geometric Methods in the Elastic Theory of Membranes in Liquid Crystal Phases*, edited by Y. B. Dai, B. L. Hao, and Z. B. Su (World Scientific, Singapore, 1999).
[17] J. R. Baumgardner and P. O. Frederickson, SIAM (Soc. Ind. Appl. Math.) J. Numer. Anal. **22**, 1107 (1985).
[18] M. F. Jarrold, Nature (London) **407**, 26 (2000).
[19] T. Kohyama, D. M. Kroll, and G. Gompper, Phys. Rev. E **68**, 061905 (2003).
[20] M. Meyer *et al.*, VisMath Proceedings, Berlin, Germany, 2002, http://multires.caltech.edu/pubsd/diffGeorOps.pdf
[21] J. Gomatam and F. Amdjadi, Phys. Rev. E **56**, 3913 (1997).
[22] D. R. Nelson, Nano Lett. **2**, 1125 (2002).
[23] M. Bowick *et al.*, Phys. Rev. Lett. **89**, 185502 (2002).
[24] I. M. Lifshitz and V. V. Slyozov, J. Phys. Chem. Solids **19**, 35 (1961).